A Fourier based numerical method for computing the dynamic permeability of periodic porous media

T.K. Nguyen, Vincent Monchiet, Guy Bonnet

A Fourier based numerical method for computing the dynamic permeability of periodic porous media

Trung-Kien Nguyen, Vincent Monchiet*, Guy Bonnet

Université Paris-Est, Laboratoire Modélisation et Simulation Multi Echelle, LMSME UMR8208 CNRS, 5 boulevard Descartes, 77454 Marne la Vallée Cedex, France

A B S T R A C T

A Fast Fourier Transform (FFT) based method for computing the dynamic permeability of periodic porous media is presented. The flow is described by the linearized Navier–Stokes equations in the presence of an oscillatory pressure gradient across the domain. The method of resolution uses an iterative scheme and exact expressions for the dynamic Green's tensor in Fourier space. The accuracy of the approach is assessed through comparisons with an exact solution, in the case of the flow in a cylindrical tube, and with available numerical data provided in the literature for the case of a flow through regular arrays of spheres or ellipsoids.

Keywords:
Porous media
Dynamic permeability
Homogenization
Fast Fourier transform
Viscous fluid

1. Introduction

The permeability of porous media is of prime importance in diverse areas of chemical and petroleum industries, civil engineering, etc. Numerous research works were effected for computing the permeability from exact or approximate images of the microstructure. For example, Sangani and Acrivos [1,2], and Wang [3] use expansions along eigenfunctions. However, these studies generally reduce their analysis to some simple geometrical configurations such as the flow through regular arrays of cylinders or spheres. For more complex microstructures, standard numerical methods, such as Finite Element, have been used for computing the permeability of porous media, such as for instance Borne et al. [4], Barrere et al. [5], Cioranescu et al. [6], Alcocer et al. [7], and Alcocer and Singh [8], Sawicki [9]. The determination of the permeability of porous media in the presence of oscillatory flow is also of great importance in many practical problems in industry and civil engineering, more specifically for characterizing the acoustic properties of porous media. From a theoretical point of view, the formulation of the boundary value problem to be solved for obtaining the dynamic permeability has been provided by using double-scale asymptotic analysis (see for instance Levy [10], Auriault et al. [11], Burridge and Keller [12], and Johnson et al. [13]). Obtaining numerical solutions of this BVP and therefore numerical values of dynamic permeability has later been the subject of studies, among which are Zhou and Sheng [14], Chapman and Higdon [15], Smeulders et al. [16], Perrot et al. [17], and Malinouskaya et al. [18]. In these approaches the authors employ semi-analytic developments or the Finite Element method.

Recently, Monchiet et al. [19] derived a Fast Fourier Transform numerical method for computing the static permeability from exact images of the microstructure. The method, first introduced by Moulinec et al. [20] for linear elastic composites, is adapted for handling problems with complex microstructures and especially digital images obtained, for example, by microtomography. Such methods are very attractive, because they are very fast, due to the use of Fast Fourier Transforms and memory-saving, using only a few variables by the discretization point instead of "stiffness matrices" containing numerous coupling terms which are used for example in the case of Finite-Element Methods. In addition, these solutions are differentiable at any order, in the same way as spectral methods (see for example [21]), all derivatives being easily obtained by using the properties of Fourier Transforms. It is worthwhile to mention that this new method can be used for computing the properties of (non-periodic) random media. Indeed, as shown by Kanit et al. [22], the periodicity conditions on the variables of the problem, which are implicit when using Fourier transforms, have been recognized as having a better convergence rate when dealing with the stochastic mean of the solutions of problems related to different samples constructed from random properties.

In this paper, we propose to extend this FFT approach, allowing the computing of the dynamic permeability of porous media.

* Corresponding author.
E-mail addresses: trungkien.nguyen@univ-paris-est.fr (T.-K. Nguyen), vincent.monchiet@univ-mlv.fr, vincent.monchiet@univ-paris-est.fr (V. Monchiet), guy.bonnet@univ-paris-est.fr (G. Bonnet).

The paper is organized as follows. In Section 2 we present the equations of the dynamic flow through a rigid periodic porous medium. In the scope of the formulation of a FFT based iterative scheme, we rewrite the problem into an equivalent one which uses a fourth order compliance tensor and we introduce the drag forces. In Section 3, the numerical approach for computing the solution of the equivalent composite problem is described. We first derive the Lippmann–Schwinger equation which is the basis of the FFT method. An iterative scheme, based on Neumann series expansion, is then formulated for the resolution of this integral equation. In the last section of the paper, we propose a validation of the approach through comparisons with existing closed-form solutions and available numerical data coming from the literature. In order to show the capacity of the method, we provide new results in the case of the dynamic flow through a regular array of ellipsoids.

2. Principle of the method

2.1. The Stokes flow

We consider a periodic porous medium saturated by a homogeneous Newtonian viscous fluid with the dynamic viscosity μ_f. The periodic medium can be represented by a parallepipedic (rectangular for 2D problems) unit cell and three vectors (2 vectors for 2D problems) of spatial invariance. We define by V_f the volume of the fluid, by V_s the volume of the rigid skeleton and by $V = V_f \cup V_s$ the total volume of the unit cell. The surface of contact between the fluid and the solid is denoted by ∂V_s. The fluid is submitted to an oscillatory macroscopic pressure gradient, of the form $\underline{\nabla} P(t) = \underline{G}\exp(i\omega t)$, where $i = \sqrt{-1}$; t is the time and ω is the radial frequency. The local velocity of the fluid is governed by the linearized Navier–Stokes equations:

$$\begin{cases} \mu_f \Delta \underline{v}(\underline{x}) + \nabla p(\underline{x}) = -i\rho_f \omega \underline{v}(\underline{x}) \quad \forall \underline{x} \in V_f \\ \operatorname{div}(\underline{v}(\underline{x})) = 0 \quad \forall \underline{x} \in V_f \\ \underline{v}(\underline{x}) = 0 \quad \forall \underline{x} \in \partial V_s \\ \underline{v}(\underline{x}) \text{ periodic}, \quad p(\underline{x}) - \underline{G}.\underline{x} \text{ periodic}. \end{cases} \tag{1}$$

In the above relations, $\underline{v}(\underline{x})$ and $p(\underline{x})$ are respectively the local velocity field and pressure. The flow of the fluid is generated by a prescribed macroscopic pressure gradient, denoted by $\underline{G}$. Consequently, the amplitude of the local pressure is decomposed as follows: $p(\underline{x}) = p^*(\underline{x}) + \underline{G}.\underline{x}$ in which $p^*(\underline{x})$ is periodic. As shown in the framework of the homogenization theory applied to porous media by Ene and Sanchez-Palencia [23], Auriault and Sanchez-Palencia [24] (see also [25]), Levy [10], Sanchez-Palencia [26], Auriault, Boutin and Geindreau [11], and Burridge and Keller [12], the macroscopic behavior is described by a generalized or "dynamic" Darcy's law:

$$\underline{V} = \langle \underline{v}(\underline{x}) \rangle_V = -\frac{1}{\mu_f} \boldsymbol{K}(\omega).\underline{G} \tag{2}$$

where $\underline{V}$ is the macroscopic velocity field and $\boldsymbol{K}(\omega)$ is a complex permeability tensor whose components depend on ω and on the size and geometry of the unit cell. It is possible to define the non-dimensional permeability by $\boldsymbol{K}^*(\omega) = \boldsymbol{K}(\omega)/S$ where S has the dimension of a surface (typically the area of the unit cell for two dimensional problems). The problem defined by Eqs. (1) presents a similitude with the problem of a periodic linear viscous composite with rigid inclusions:

$$\begin{cases} \dot{\underline{\varepsilon}}(\underline{x}) = \dfrac{1}{2}(\nabla \underline{v}(\underline{x}) + \nabla^t \underline{v}(\underline{x})) \quad \forall \underline{x} \in V \\ \dot{\underline{\varepsilon}}(\underline{x}) = \mathbb{S}(\underline{x}) : \sigma(\underline{x}) \quad \forall \underline{x} \in V \\ \operatorname{div}(\sigma(\underline{x})) + \underline{f}(\underline{x}) = -i\rho_f \omega \underline{v}(\underline{x}) \quad \forall \underline{x} \in V \\ \sigma(\underline{x}).\underline{n} \quad \text{antiperiodic} \\ \underline{v}(\underline{x}) \quad \text{periodic}. \end{cases} \tag{3}$$

In the above equations, $\dot{\underline{\varepsilon}}(\underline{x}) = \underline{\nabla}_s \underline{v}(\underline{x})$ represents the local strain rate while $\underline{\nabla}_s$ is the symmetric gradient operator, $\sigma(\underline{x})$ is the local stress. Both $\dot{\underline{\varepsilon}}(\underline{x})$ and $\sigma(\underline{x})$ are periodic and their volumic mean over the unit cell is null: $\langle \dot{\underline{\varepsilon}}(\underline{x}) \rangle_V = 0$ and $\langle \sigma(\underline{x}) \rangle_V = 0$. The FFT based method is employed for solving the equations of the equivalent linear viscous composite. Since this Fourier based method uses a description of the unit cell by a finite number of points taken along a regular grid, a continuation by continuity of the local fields within the rigid inclusions is required. In (3) the following expression for the fourth order tensor $\mathbb{S}(\underline{x})$ is then considered:

$$\mathbb{S}(\underline{x}) = \frac{1}{2\mu(\underline{x})}\mathbb{K} \quad \text{with} : \mu(\underline{x}) = \begin{cases} \mu_f & \forall \underline{x} \in V_f \\ +\infty & \forall \underline{x} \in V_s \end{cases} \tag{4}$$

where $\mathbb{K} = \mathbb{I} - \mathbb{J}$ with $\mathbb{J} = \frac{1}{3}\boldsymbol{I} \otimes \boldsymbol{I}$ where $\mathbb{I}$ is the fourth order identity tensor while $\boldsymbol{I}$ is the second order identity tensor. Note that in Eqs. (3), the local stress contains a deviatoric and a spherical part. However, due to the property $\mathbb{K} : \boldsymbol{I} = 0$, the incompressibility ($\operatorname{tr}(\dot{\underline{\varepsilon}}) = 0$) is recovered within the fluid. On the other hand, since the dynamic viscosity tends to infinity in the solid phase, the strain rate is null, which is consistent with the condition of non-deformability of the skeleton. The flow is generated by a given "macroscopic" gradient of pressure. For studying the periodic part, considered as the fluctuation of the flow at the microscopic scale, this macroscopic gradient of pressure can be interpreted as a given body force through the fluid phase, which must be extended toward the solid phase for solving the problem within the two phase cell:

$$\underline{f}(\underline{x}) = \begin{cases} \underline{G} & \forall \underline{x} \in V_f \\ ? & \forall \underline{x} \in V_s. \end{cases} \tag{5}$$

In the above expression, the body force is undetermined within the solid phase (in V_s). Body forces in V_s are however required in order to equilibrate the traction acting on the surface of the solid. This point is discussed in the next section.

Note that the description of the body forces acting within the solid phase is inherent with the use of a FFT based algorithm. Indeed, when the Finite Element Method (FEM), for example, is employed for solving the Stokes equations, only the fluid phase is meshed. The surface ∂V_s is considered as the domain boundary on which the Dirichlet condition, $\underline{v} = 0$, is applied. The FFT based method uses the discrete Fourier transform and therefore a regular meshing on the periodic cell. The points of that grid are located within the fluid or the solid phase and a continuation by continuity of the mechanical fields within the solid phase is then effected. Particularly, this require a continuation by continuity of the mechanical fields but also the introduction of body forces within the solid phase. Note also that the solid/fluid interface is not modeled with the FFT algorithm (again, due to the consideration of a regular meshing) and the condition of adherence is not explicitly implemented. In fact, the adherence conditions are implicitly verified by considering body forces in the solid phase which must be chosen adequately in order to fix the solid.

2.2. Body forces within the solid and elementary problems for the determination of the permeability tensor

In this subsection we present the method for computing the body forces acting within the solid phase as well as the elementary problems to be solved for obtaining the components of the permeability tensors. As explained before, the forces acting within the solid phase must be identified, so that the problem of the equivalent composite (3) will be well-posed.

In (3), the strain rate field $\dot{\underline{\varepsilon}}(\underline{x})$ is null within the solid phase. The velocity field coming by integration of the strain rate field is then defined up to an added rigid displacement of each unconnected

solid. We assume that the unit cell contains M distinct solids centered at $\underline{x} = \underline{X}^{(i)}$ for $i = 1..M$. For many situations, the skeleton of the porous medium is a connected solid. However, it is very useful to provide validations for plane flow which lead obviously to studying a solid phase constituted of non-connected solids. It is the same for 3D computations related to non-connected spherical particles distributed along periodic networks, which are used either for validation of some numerical solutions or for providing estimations of permeability through suspensions.

Let us consider such an assembly of unconnected solids. The volumes of the solids are denoted by V_{si} for $i = 1..M$ and the total volume of the solid phase is denoted by $V_s = V_{s1} \cup V_{s2} \cup \cdots \cup V_{sM}$. The velocity field coming by integration within the inclusion i, has the following general form:

$$\underline{v}(\underline{x}) = \underline{V}^{(i)} + \underline{\Omega}^{(i)} \wedge (\underline{x} - \underline{X}^{(i)}) \tag{6}$$

where $\underline{V}^{(i)}$ and $\underline{\Omega}^{(i)}$ are respectively the translational and angular velocities of the inclusion i. The values of $\underline{V}^{(i)}$ and $\underline{\Omega}^{(i)}$ are evaluated by computing the translational and angular velocity fields for a point taken within the solid i. If one considers that the assembly of these solids acts as a porous medium, it is necessary to consider that these inclusions are fixed. In order to fix these inclusions, body forces, interpreted as forces and couples, are introduced. Within a solid located at $\underline{x} = \underline{X}^{(i)}$, the expression of $\underline{f}(\underline{x})$ is then taken as:

$$\underline{f}(\underline{x}) = \underline{F}^{(i)} + \underline{C}^{(i)} \wedge (\underline{x} - \underline{X}^{(i)}). \tag{7}$$

Since the stress field is periodic, the equilibrium of the unit cell reduces to $\langle \underline{f}(\underline{x}) \rangle_V = -i\omega\rho_f \underline{V}$ which also reads:

$$\phi_f \underline{G} + \sum_{i=1}^{i=M} \phi_{si} \underline{F}^{(i)} = -i\omega\rho_f \underline{V} \tag{8}$$

where $\phi_f = V_f/V$ is the porosity and $\phi_{si} = V_{si}/V$.

Due to the linearity of the equations of the problem, its solution linearly depends on the loading parameter $\underline{G}$ and on the drag forces $\underline{F}^{(i)}$ and $\underline{C}^{(i)}$ for $i = 1..M$ (see Fig. 1). Particularly, by integrating the strain rate field $\dot{\boldsymbol{\varepsilon}}(x)$, the velocity field reads:

$$\underline{v}(\underline{x}) = \underline{V} + \boldsymbol{A}(\underline{x}).\underline{G} + \sum_{s=1}^{s=M} \left[\boldsymbol{L}_s(\underline{x}).\underline{F}^{(s)} + \boldsymbol{M}_s(\underline{x}).\underline{C}^{(s)} \right] \tag{9}$$

where $\underline{V}$ is the macroscopic velocity field, and the localization tensors $\boldsymbol{A}(\underline{x})$, $\boldsymbol{L}_r(\underline{x})$, $\boldsymbol{M}_r(\underline{x})$ are periodic and have a zero volume average: $\langle \boldsymbol{A}(\underline{x}) \rangle_V = \langle \boldsymbol{L}_r(\underline{x}) \rangle_V = \langle \boldsymbol{M}_r(\underline{x}) \rangle_V = 0$. The angular velocity $\underline{\omega}(\underline{x}) = \frac{1}{2}\mathrm{rot}\underline{v}(\underline{x})$ reads:

$$\underline{\omega}(\underline{x}) = \boldsymbol{B}(\underline{x}).\underline{G} + \sum_{s=1}^{s=M} \left[\boldsymbol{P}_s(\underline{x}).\underline{F}^{(s)} + \boldsymbol{Q}_s(\underline{x}).\underline{C}^{(s)} \right] \tag{10}$$

where the localization tensors $\boldsymbol{B}(\underline{x})$, $\boldsymbol{P}_s(\underline{x})$, $\boldsymbol{Q}_s(\underline{x})$ are periodic and have a zero volume average: $\langle \boldsymbol{B}(\underline{x}) \rangle_V = \langle \boldsymbol{P}_s(\underline{x}) \rangle_V = \langle \boldsymbol{Q}_s(\underline{x}) \rangle_V = 0$. The translational and angular velocities defined in Eq. (6) are then computed by:

$$\begin{cases} \underline{V}^{(r)} = \underline{v}(\underline{x} = \underline{X}^{(r)}) = \underline{V} + \boldsymbol{A}_r.\underline{G} + \displaystyle\sum_{s=1}^{s=M} \left[\boldsymbol{L}_{rs}.\underline{F}^{(s)} + \boldsymbol{M}_{rs}.\underline{C}^{(s)} \right] \\ \underline{\Omega}^{(r)} = \underline{\omega}(\underline{x} = \underline{X}^{(r)}) = \boldsymbol{B}_r.\underline{G} + \displaystyle\sum_{s=1}^{s=M} \left[\boldsymbol{P}_{rs}.\underline{F}^{(s)} + \boldsymbol{Q}_{rs}.\underline{C}^{(s)} \right] \end{cases} \tag{11}$$

with:

$$\begin{cases} \boldsymbol{A}_r = \boldsymbol{A}(\underline{x} = \underline{X}^{(r)}), & \boldsymbol{B}_r = \boldsymbol{A}(\underline{x} = \underline{X}^{(r)}) \\ \boldsymbol{L}_{rs} = \boldsymbol{L}_s(\underline{x} = \underline{X}^{(r)}), & \boldsymbol{M}_{rs} = \boldsymbol{M}_s(\underline{x} = \underline{X}^{(r)}) \\ \boldsymbol{P}_{rs} = \boldsymbol{P}_s(\underline{x} = \underline{X}^{(r)}), & \boldsymbol{Q}_{rs} = \boldsymbol{Q}_s(\underline{x} = \underline{X}^{(r)}). \end{cases} \tag{12}$$

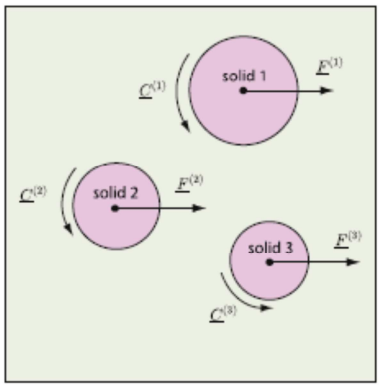

Fig. 1. Schematic illustrating the drag force.

The solids being fixed, the translational and angular velocities given by (11) must be zero. It leads to:

$$\begin{cases} \underline{V} + \boldsymbol{A}_r.\underline{G} + \displaystyle\sum_{s=1}^{s=M} \left[\boldsymbol{L}_{rs}.\underline{F}^{(s)} + \boldsymbol{M}_{rs}.\underline{C}^{(s)} \right] = 0 \quad \text{for: } r = 1..M \\ \boldsymbol{B}_r.\underline{G} + \displaystyle\sum_{s=1}^{s=M} \left[\boldsymbol{P}_{rs}.\underline{F}^{(s)} + \boldsymbol{Q}_{rs}.\underline{C}^{(s)} \right] = 0 \quad \text{for: } r = 1..M. \end{cases} \tag{13}$$

The above equations together with Eq. (8) lead to a linear system of dimension $6M + 3$ for the unknowns: $\underline{V}, \underline{F}^{(i)}$ and $\underline{C}^{(i)}$ for $i = 1..M$. The determination of all coefficients which enter into that linear system, namely the components of $\boldsymbol{A}_r$, $\boldsymbol{B}_r$, $\boldsymbol{L}_{rs}$, $\boldsymbol{M}_{rs}$, $\boldsymbol{P}_{rs}$ and $\boldsymbol{Q}_{rs}$, requires the computation of the localization tensors which enter into (9) and (10). This is effected by solving a total number of $6M+3$ elementary problems associated to each component of $\underline{G}, \underline{F}^{(i)}$ and $\underline{C}^{(i)}$. In the next section we propose a FFT based computational method for the resolution of these elementary problems. It must be emphasized that the method previously described allows us to effect the computation of the dynamic permeability in any case. However, in the simplest cases, symmetry properties allow us to reduce drastically the number of computations (this is the case for the examples considered in Section 4).

3. The FFT based iterative scheme

In this section we provide an algorithm for computing the localization tensors which appear within the definition of the translational and angular velocity fields $\underline{v}(\underline{x})$ and $\underline{\omega}(\underline{x})$, given by relations (9) and (10) respectively. The method is inspired by the original FFT based approach initially proposed by Moulinec and Suquet [20] and its dual formulation [27,28]. The iterative scheme developed in [20] for linear elastic composites is strain based and uses the rigidity tensor. It has been earlier shown that this method diverges in the case of rigid inclusion (see for instance [29,30]) since the rigidity tends to infinity in the inclusion. A stress based formulation [27,28] is more suitable for handling the problem of composites with rigid inclusions since it uses the compliance tensor which has zero components in the rigid phase. In the present section we then propose a stress based iterative scheme which uses the dynamic Green operator to take into account the inertia terms. We also mention that the proposed algorithm for porous media differs from the one used for composites by the first term of the series which depends on the body forces $\underline{f}(\underline{x})$.

In the following section, we first establish the Lippmann–Schwinger integral equation for the problem of dynamic flow which is the basis of the proposed iterative scheme.

3.1. The integral equation for the strain rate

In this section we propose to derive the Lippmann–Schwinger integral equation for the dynamic flow, which is, in fact, the basis of the formulation of the FFT based iterative scheme. The first step for the derivation of this integral equation consists in introducing into relations (3) a reference medium of viscosity μ_0 and the eigenstrain $\underline{\eta}(\underline{x}) = (\mathbb{S}(\underline{x}) - \mathbb{S}^0) : \underline{\sigma}(\underline{x})$ with $\mathbb{S}^0 = 1/(2\mu_0)\mathbb{K}$. In the Fourier space, the system of Eqs. (3) becomes:

$$\begin{cases} \underline{\dot{\varepsilon}}(\underline{\xi}) = i\underline{v}(\underline{\xi}) \overset{s}{\otimes} \underline{\xi} \\ \underline{\dot{\varepsilon}}(\underline{\xi}) = \mathbb{S}^0 : \underline{\sigma}(\underline{\xi}) + \underline{\eta}(\underline{\xi}) \\ i\underline{\sigma}(\underline{\xi}).\underline{\xi} + \underline{f}(\underline{\xi}) = -i\rho_f \omega \underline{v}(\underline{\xi}). \end{cases} \tag{14}$$

In the above equations, $\underline{v}(\underline{\xi}), \underline{\dot{\varepsilon}}(\underline{\xi}), \underline{\sigma}(\underline{\xi}), \underline{f}(\underline{\xi})$ represent the Fourier transforms of the quantities $\underline{v}(\underline{x}), \underline{\dot{\varepsilon}}(\underline{x}), \underline{\sigma}(\underline{x}), \underline{f}(\underline{x})$. When $\underline{\eta}(\underline{\xi})$ is given, the resolution of (14) becomes straightforward. Indeed, from the first two relations in (14), one can eliminate the strain rate $\underline{\dot{\varepsilon}}(\underline{\xi})$; it gives:

$$\underline{\sigma}(\underline{\xi}) = p(\underline{\xi})\boldsymbol{I} + 2\mu_0\left[i\underline{v}(\underline{\xi}) \overset{s}{\otimes} \underline{\xi} - \underline{\eta}(\underline{\xi})\right] \tag{15}$$

where it is recalled that $p(\underline{\xi})$ is the pressure, $p(\underline{\xi}) = \mathrm{tr}(\underline{\sigma}(\underline{\xi}))/3$. Introducing this equation into the last one in (14) and taking into account the incompressibility, $\underline{v}(\underline{\xi}).\underline{\xi} = 0$, we obtain:

$$-\mu_0|\underline{\xi}|^2(1-\kappa)\underline{v}(\underline{\xi}) + ip(\underline{\xi})\underline{\xi} = -\underline{f}(\underline{\xi}) + 2i\mu_0\underline{\eta}(\underline{\xi}).\underline{\xi} \tag{16}$$

in which the non-dimensional parameter $\kappa = i\rho_f\omega/(\mu_0|\underline{\xi}|^2)$ has been introduced. Using again the incompressibility condition, it is possible to derive, from the above equation, the expressions of both velocity field and pressure:

$$\begin{cases} p(\underline{\xi}) = \dfrac{i}{|\underline{\xi}|^2}\underline{f}.\underline{\xi} + 2\mu_0\underline{\eta}(\underline{\xi}) : \boldsymbol{k} \\ \underline{v}(\underline{\xi}) = \dfrac{1}{\mu_0|\underline{\xi}|^2(1-\kappa)}\boldsymbol{k}^\perp.\underline{f} \\ \qquad\quad - \dfrac{2i}{|\underline{\xi}|^2(1-\kappa)}\left[\underline{\eta}(\underline{\xi}).\underline{\xi} - \underline{\xi}(\underline{\eta}(\underline{\xi}) : \boldsymbol{k})\right] \end{cases} \tag{17}$$

where the following notations have been used:

$$\boldsymbol{k} = \frac{1}{|\underline{\xi}|^2}\underline{\xi} \otimes \underline{\xi}, \qquad \boldsymbol{k}^\perp = \boldsymbol{I} - \boldsymbol{k}. \tag{18}$$

Introducing now the expressions (17) into relation (15), we find for the stress field:

$$\underline{\sigma}(\underline{\xi}) = \underline{\varphi}(\underline{\xi}, \kappa) - \underline{\boldsymbol{\Delta}}^0(\underline{\xi}, \kappa) : \underline{\eta}(\underline{\xi}) \tag{19}$$

in which the second order tensor $\underline{\varphi}(\underline{\xi}, \kappa)$ is given by:

$$\underline{\varphi}(\underline{\xi}, \kappa) = \frac{2i}{|\underline{\xi}|^2(1-\kappa)}\left[\underline{f}(\underline{\xi}) \overset{s}{\otimes} \underline{\xi} - \underline{f}(\underline{\xi}).\underline{\xi}\boldsymbol{k}\right] + \frac{i}{|\underline{\xi}|^2}\boldsymbol{I}\underline{f}.\underline{\xi} \tag{20}$$

when $\underline{\xi} \neq 0$ but $\underline{\varphi}(\underline{\xi}, \kappa) = 0$ for $\underline{\xi} = 0$. In expression (19), $\underline{\boldsymbol{\Delta}}^0(\underline{\xi}, \kappa)$ is a fourth order tensor defined by:

$$\underline{\boldsymbol{\Delta}}^0(\underline{\xi}, \kappa) = 2\mu_0\left[\boldsymbol{k}^\perp \otimes \boldsymbol{k}^\perp + \boldsymbol{k}^\perp \underline{\otimes} \boldsymbol{k}^\perp + \frac{\kappa}{1-\kappa}(\boldsymbol{k}^\perp \underline{\otimes} \boldsymbol{k} + \boldsymbol{k} \underline{\otimes} \boldsymbol{k}^\perp)\right] \tag{21}$$

when $\underline{\xi} \neq 0$ and $\underline{\boldsymbol{\Delta}}^0(\underline{\xi}, \omega) = 0$ for $\underline{\xi} = 0$. The tensor $\underline{\boldsymbol{\Delta}}^0(\underline{\xi}, \kappa)$ is the dynamic Green operator for the stress. When $\kappa = 0$, one recovers the expression of the static Green tensor for the stress and for an incompressible medium: $2\mu_0\left[\boldsymbol{k}^\perp \otimes \boldsymbol{k}^\perp + \boldsymbol{k}^\perp \underline{\otimes} \boldsymbol{k}^\perp\right]$ (see for instance [30] which uses the same notations as the ones used in the present paper). In (21), the following notation has been used (for any couple of second order tensors $\boldsymbol{a}$ and $\boldsymbol{b}$):

$$(\boldsymbol{a} \underline{\otimes} \boldsymbol{b})_{ijkl} = \frac{1}{2}(a_{ik}b_{jl} + a_{il}b_{jk}). \tag{22}$$

The details about the calculation of $\underline{\varphi}(\underline{\xi}, \kappa)$ and $\underline{\boldsymbol{\Delta}}^0(\underline{\xi}, \kappa)$ can be found in the Appendix A. The integral equation is then obtained by replacing, in (19), the expression of the eigenstrain as a function of the stress field:

$$\underline{\sigma}(\underline{\xi}) = \underline{\varphi}(\underline{\xi}, \kappa) - \underline{\boldsymbol{\Delta}}^0(\underline{\xi}, \kappa) : \left[\mathbb{S}(\underline{\xi}) * \underline{\sigma}(\underline{\xi}) - \mathbb{S}^0 : \underline{\sigma}(\underline{\xi})\right] \tag{23}$$

or, equivalently:

$$\underline{\sigma}(\underline{x}) = \underline{\varphi}(\underline{x}, \kappa) - \underline{\boldsymbol{\Delta}}^0(\underline{x}, \kappa) * \left[(\mathbb{S}(\underline{x}) - \mathbb{S}^0) : \underline{\sigma}(\underline{x})\right]. \tag{24}$$

In relations (23) and (24), the symbol "$*$" denotes the convolution product.

3.2. The algorithm

Following Moulinec and Suquet [20] and later Bhattacharya and Suquet [27], and Bonnet [28] for the stress based formulation, the solution of the integral equation (23) or equivalently (24) is expanded along Neumann series. Each term of that series is obtained by means of the following recurrence relation:

$$\underline{\sigma}^{r+1}(\underline{x}) = \underline{\varphi}(\underline{x}, \kappa) - \underline{\boldsymbol{\Delta}}^0(\underline{x}, \kappa) * \left[(\mathbb{S}(\underline{x}) - \mathbb{S}^0) : \underline{\sigma}^r(\underline{x})\right] \tag{25}$$

which is initiated by:

$$\underline{\sigma}^{r=1}(\underline{\xi}) = \underline{\varphi}(\underline{x}, \kappa). \tag{26}$$

The exact Fourier transform is thereafter replaced by the discrete Fourier transform. The discrete wave vectors, $\underline{\xi}_n$, are taken from $n = -N$ to $n = N-1$, and by $\underline{x}_n$ we denote the position of the nodes of the regular grid in real space. The compliance $\mathbb{S}(\underline{x}_n)$ is then computed at each node of that grid from the exact images of the microstructures. The algorithm is summarized below:

$$\begin{aligned} &\underline{\sigma}^r(\underline{x}_n) = \mathcal{F}^{-1}(\underline{\sigma}^r(\underline{\xi}_n)) \\ &\underline{\dot{\varepsilon}}^r(\underline{x}_n) = \mathbb{S}(\underline{x}_n) : \underline{\sigma}^r(\underline{x}_n) \\ &\underline{\dot{\varepsilon}}^r(\underline{\xi}_n) = \mathcal{F}(\underline{\dot{\varepsilon}}^r(\underline{x}_n)) \\ &\text{convergence test} \\ &\underline{\sigma}^{r+1}(\underline{\xi}_n) = \underline{\varphi}(\underline{\xi}_n, \kappa) \\ &\qquad - \underline{\boldsymbol{\Delta}}^0(\underline{\xi}_n, \kappa) : \left[\underline{\dot{\varepsilon}}^l(\underline{\xi}_n) - \mathbb{S}^0 : \underline{\sigma}^l(\underline{\xi}_n)\right]. \end{aligned} \tag{27}$$

In (27), $\mathcal{F}$ and $\mathcal{F}^{-1}$ denote the Fourier Transform and its inverse for which the FFT algorithm is employed. The following convergence test is used:

$$\frac{\|\underline{\dot{\varepsilon}}^{r+1}(\underline{\xi}_n) - \underline{\dot{\varepsilon}}^r(\underline{\xi}_n)\|}{\|\underline{\dot{\varepsilon}}^{r+1}(\underline{\xi}_n)\|} < \epsilon. \tag{28}$$

In (28), $\|\bullet\|$ denotes the Frobenius norm and the value $\epsilon = 10^{-3}$ is used in the present work.

At convergence of the iterative scheme, one can compute the velocity associated to the strain rate field $\underline{\dot{\varepsilon}}^l(\underline{\xi}_n)$. Using the incompressibility condition ($\underline{v}(\underline{\xi}_n).\underline{\xi}_n = 0$), one has:

$$\begin{cases} \underline{v}(\underline{\xi}) = -\dfrac{2i}{|\underline{\xi}|^2}\underline{\dot{\varepsilon}}(\underline{\xi}).\underline{\xi} & \text{for } \underline{\xi} \neq 0 \\ \underline{v}(\underline{\xi}) = 0 & \text{for } \underline{\xi} = 0. \end{cases} \tag{29}$$

The rotational velocity $\underline{\omega}(\underline{\xi})$ is:

$$\begin{cases} \underline{\omega}(\underline{\xi}) = \dfrac{1}{2}\underline{\xi} \wedge \underline{v}(\underline{\xi}) & \text{for } \underline{\xi} \neq 0 \\ \underline{\omega}(\underline{\xi}) = 0 & \text{for } \underline{\xi} = 0. \end{cases} \tag{30}$$

The inverse Fourier transform is thereafter used for computing the translational and angular velocities $\underline{v}(\underline{x})$ and $\underline{\omega}(\underline{x})$ and then the localization tensor in expressions (9) and (10). In the next section, we propose to validate the FFT based approach by comparison with existing results coming from the literature. Moreover new results are also provided in the case of a regular network of ellipsoidal inclusions.

4. Validations

4.1. The flow in a cylindrical tube

As a first step of the validation of the FFT based approach, we compare our results with an existing closed-form solution in the particular case of the flow through an array of cylindrical tubes of radius a. The considered periodic porous medium is then defined by an array of cylinders, aligned along the direction Ox_3, and we denote by $2b$ the distance between two neighboring cylindrical tubes. The flow is generated by applying the gradient of pressure G_3. The closed-form expressions for the velocity field as well as the permeability have been already derived in [31,14,25]. The only non-null component of the permeability tensor is K_{33} and its expression is:

$$K_{33} = \frac{ia}{\omega b^2}\left(a - \frac{2}{\sqrt{i\omega}}\frac{J_1(\sqrt{i\omega}a)}{J_0(\sqrt{i\omega}a)}\right). \tag{31}$$

In which $J_n(x)$ denotes the Bessel function of the first kind and order n. This exact solution is now compared with the numerical one. For computing the permeability K_{33} with the FFT based iterative scheme we choose a squared unit cell, having the width $2b$, and containing a circular subdomain of radius a which contains the fluid of viscosity μ_f. Due to the symmetry of the problem, a constant body force $f_3 = F_3$ is considered within the solid phase. So, the permeability $K(\omega)$ is obtained after the resolution of two elementary problems defined by:

$$\begin{cases} \text{Loading case 1: } G_3 = 1, & F_3 = -\phi_f/\phi_s & V_3 = 0 \\ \text{Loading case 1: } G_3 = 0, & F_3 = -i\omega/\phi_s, & V_3 = 1 \end{cases} \tag{32}$$

where $\phi_f = \pi a^2/(4b^2)$ is the volume fraction of the fluid and $\phi_s = 1 - \phi_f$ is the volume fraction of the solid. In the case of the first loading, a gradient of pressure $G_3 = 1$ is applied within the fluid phase and the force $F_3 = -\phi_f/\phi_s$ is applied within the solid phase to obtain the equilibrium of the cell (according to Eq. (8)). The velocity field associated with this first loading has a null volume average over the unit cell. In the case of the second loading, the velocity field has the mean velocity $V_3 = 1$ while the gradient of pressure $G_3 = 0$ is applied within the fluid. To obtain the equilibrium of the cell, the body force acting within the solid phase is chosen as $F_3 = -i\omega/\phi_s$. For each elementary problem, the flow generates a velocity of the solid, denoted V_3^s. This velocity depends on the two parameters G_3, V_3 (F_3 being related to these parameters due to the equilibrium of the cell):

$$V_3^s = AG_3 + BV_3. \tag{33}$$

The solution of (1) corresponds to V_3^s which leads to $V_3 = -BG_3/A$ and then, according to the Darcy law (2), the longitudinal permeability is $K_{33} = \mu_f B/A$.

In Fig. 2 we show the variations of the real part and of the imaginary part of the non-dimensional dynamic permeability K_{33}/S as functions of the non-dimensional frequency $\overline{\omega} = \omega S\mu_f$ where $S = 4b^2$ is the area of the unit cell and the radius a of the tube is obtained from the ratio $a/b = 0.4$. As already shown in [32,14] the real part of the dynamic permeability is constant for low values of the frequency ω but linearly decreases with ω, at large frequencies (in a log–log frame). The full line represents the exact solution while the discrete points refer to the FFT based numerical data. For the numerical solution, a grid containing 256×256 points has been considered to obtain a good accuracy of the numerical results.

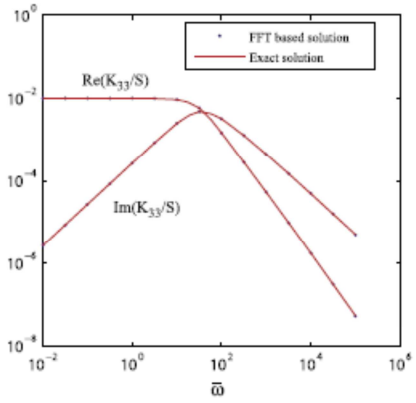

Fig. 2. The real part and the imaginary part of the non-dimensional permeability K_{33}/S (with $S = \pi a^2$) for the flow through a circular tube of radius a.

Table 1
The real part, $Re(K_{33})/S$, and the imaginary part, $Im(K_{33})/S$, of the non-dimensional permeability K_{33}/S (with $S = \pi a^2$) for the flow through an array of circular tubes of radius a. These values are given for $a/b = 0.4$, $\overline{\omega} = 10^{-2}$ and for diverse values of the resolution.

Resolution	$Re(K_{33})/S$	Error (%)	$Im(K_{33})/S(\times 10^{-6})$	Error (%)
16×16	0.0100825	0.292	2.68958	0.326
32×32	0.0100535	0.044	2.680994	0.006
64×64	0.0100554	0.023	2.681496	0.025
128×128	0.0100552	0.021	2.681339	0.019
256×256	0.0100548	0.017	2.680881	0.002

For completeness, we investigate the convergence of the FFT based solution with the resolution (in fact the number of wave vectors used for performing the Fourier transform and its inverse). In Table 1, we provide the values of the real part and of the imaginary part of the non-dimensional permeability as functions of the resolution. We also give the relative error of the FFT based solution as compared with the exact solution. Table 2 displays the same results for the case $\overline{\omega} = 10^4$. It can be observed that, for low values of the frequency (Table 1), the error induced for the real part as well as for the complex part is inferior to 0.1% when a grid 16×16 is used.

For larger values of the frequency (Table 2), one can observe an increase of the error (for a given wave number discretization) by comparison with the values reported in Table 1. This increase is attributed to the formation of a boundary layer at the vicinity of the surface of the solid, whose thickness decreases with frequency. Indeed, the pixels are squared with the width $b/128 \simeq 0.0078b$ (where it is recalled that b is the half width of the unit cell). On the other hand, the thickness of the boundary layer is $\lambda = \sqrt{\frac{\mu_f}{\rho_f \omega}} = \frac{2b}{\sqrt{\overline{\omega}}}$. Particularly, when $\overline{\omega} = 10^{-2}$ the boundary effects vanishes since $\lambda = 20b$ while for $\overline{\omega} = 10^4$, the thickness of the boundary layer is $\lambda = 0.02b$. The error, which is reported on Table 2, is

Table 2
The real part, $Re(K_{33})/S$, and the imaginary part, $Im(K_{33})/S$, of the non-dimensional permeability K_{33}/S (with $S = \pi a^2$) for the flow through a circular tube of radius a. These values are given for $a/b = 0.4$, $\overline{\omega} = 10^4$ and for diverse values of the resolution.

Resolution	$Re(K_{33})/S$	Error (%)	$Im(K_{33})/S$	Error (%)
16×16	0,0187798	7,049	0,490081	1,061
32×32	0,0166513	4,832	0,483854	0,212
64×64	0,0171832	1,587	0,484789	0,019
128×128	0,0173526	0,595	0,484879	0,0005
256×256	0,0174716	0,090	0,48488	0,0002

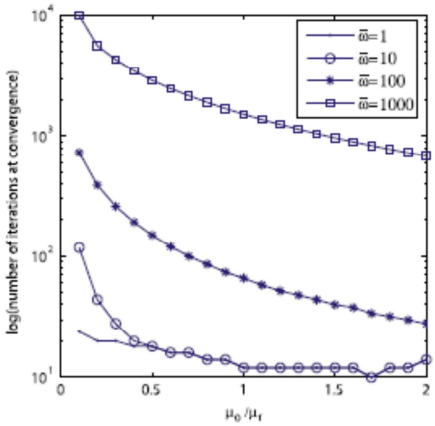

Fig. 3. Number of iterations at convergence of the iterative scheme as a function of μ_0/μ_f and for various values of ω.

inferior to 10^{-3} when the resolution is 256×256. Based on that observation, for the 3D calculations provided in the next section, the resolution $256 \times 256 \times 256$ has been considered.

For completeness we now discuss the choice of the modulus μ_0 of the reference medium. In Fig. 3, we represent the number of iterations at convergence of the iterative scheme as a function of the ratio μ_0/μ_f and for various values of ω. First, the representation is restricted to the interval $]0, 2]$ since for other values of the ratio μ_0/μ_f the iterative scheme diverges. In the range $]0, 2]$ the numerical results show that the optimal choice for μ_0 (leading to the lowest number of iterations at convergence) is close to $\mu_0 = 2\mu_f$. This value has been chosen for providing the above numerical results and also those proposed in the next section. There must also be noted a diminution of the rate of convergence of the iterative scheme when increasing the values of ω. It implies that the problem with high values of the frequency is computationally costly as compared to the static case ($\omega = 0$).

4.2. Flow through regular networks of spheres and ellipsoids

As a second validation we propose to compute the dynamic permeability in the case of three-dimensional flows through networks of spheres. The basic cell is cubic, with the width $2b$, and contains a sphere of radius a. Due to the geometry of the unit cell, the permeability tensor is isotropic and can be put into the form $\boldsymbol{K}(\omega) = K(\omega)\boldsymbol{I}$ where it is recalled that $\boldsymbol{I}$ is the identity tensor. The computation of $K(\omega)$ is performed by applying to the unit cell the component of the gradient of pressure G_1 and by computing the only non-null component of the macroscopic velocity field V_1. As in the previous case, due to the symmetry of the unit cell, the body force acting within the solid phase is chosen as $f_1 = F_1$ and other components f_2 and f_3 are taken as zero. The method

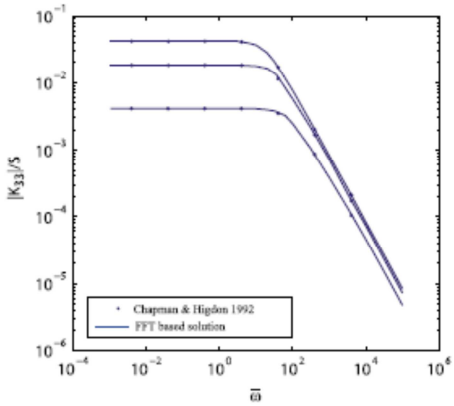

Fig. 4. Magnitude of the non-dimensional permeability, $|K|/S$, as a function of the non-dimensional frequency $\overline{\omega}$ in the case of an array of spheres and for various values of the volume fraction of the solid phase, ϕ_s. From the top, $\phi_s = 0.125, 0.216, 0.450$.

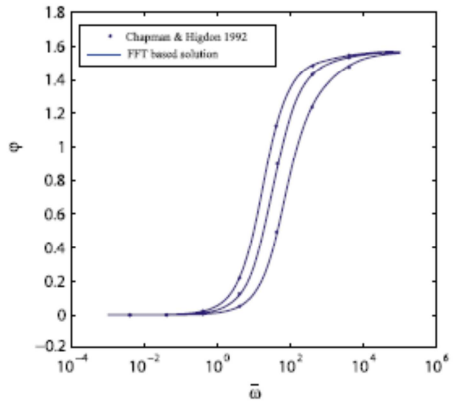

Fig. 5. The phase $\varphi = \arctan(K_R/K_I)$ (where K_R and K_I are the real and imaginary parts of the permeability K), as a function of the non-dimensional frequency $\overline{\omega}$ in the case of an array of spheres and for various values of the volume fraction of the solid phase, ϕ_s. From the top, $\phi_s = 0.125, 0.216, 0.450$.

for computing the permeability, described in the general case in Section 2.2, appears here to be very similar to the case of the tube, studied in the last section.

Fig. 4 represents the magnitude of the non-dimensional permeability, $|K|/S$, as a function of the non-dimensional frequency $\overline{\omega}$ in the case of an array of spheres and for various values of the volume fraction of the solid phase, $\phi_s = (4/3\pi a^3)/(8b^3)$. In Fig. 5 is plotted the phase $\varphi = \arctan(K_R/K_I)$, where K_R and K_I are the real and imaginary parts of the permeability K, as functions of the non-dimensional frequency $\overline{\omega}$ in the case of a network of spheres and for various values of the volume fraction of the solid phase, ϕ_s. The full lines correspond to the solution computed by the FFT based iterative scheme while the discrete points are results obtained from series expansion by Chapman and Higdon [15]. It can be noticed that our results are in good agreement with the ones of Chapman and Higdon [15].

In order to investigate the role of the pore geometry we consider the case of a three-dimensional flow through a regular array of ellipsoids. The unit cell is described in Fig. 6. It is cuboidal and contains an ellipsoid of semi-axes a_1, a_2 and a_3 aligned with the

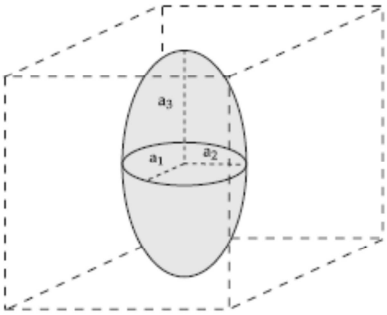

Fig. 6. The unit cell of the periodic array of ellipsoidal inclusions.

cartesian axes Ox_1, Ox_2 and Ox_3 respectively. The volume of the inclusion is $V_s = 4\pi a_1 a_2 a_3/3$ and the porosity is $f = 1 - 4/3\pi\, a_1 a_2\, a_3/(8b^8)$ (b being the half-width of the basic cell) when the inclusions are not interpenetrable. The permeability tensor is orthotropic and has the following non-zero components: $K_{11}(\omega)$, $K_{22}(\omega)$ and $K_{33}(\omega)$.

The semi-axes of the ellipsoid are chosen as follows: $a_1 = a_2 = R/\epsilon^{1/3}$ and $a_3 = \epsilon^{2/3}R$ where $\epsilon = a_3/a_1$ is the aspect ratio of the ellipsoid and R is the radius of the sphere corresponding to an aspect ratio $\epsilon = 1$. The porosity is then given by $f = 1 - 4/3\pi R^3/(8b^3)$ and is independent of the aspect ratio ϵ. For our numerical applications, $R = b/2$ and the value of the aspect ratio is taken in the range $[1/8, 2\sqrt{2}]$. The case $\epsilon = 1/8$ corresponds to a flat spheroid with the semi-axes $a_1 = a_2 = b$ and $a_3 = b/8$. The case $\epsilon = 2\sqrt{2}$ corresponds to a prolate spheroidal inclusion with the semi-axes $a_1 = a_2 = b/(2\sqrt{2})$ and $a_3 = b$. The value of the aspect ratio is restricted to the interval $[1/8, 2\sqrt{2}]$ since for other values the condition of non-interpenetration is not verified and the porosity does not remain independent of the aspect ratio. In Fig. 7 we represent the magnitude of the non-dimensional permeability, $|K_{33}|/S$ as a function of the aspect ratio for different values of the non-dimensional frequency $\overline{\omega} = 1, 10, 100, 1000$. Fig. 8 displays similar results for the phase $\varphi = \arctan(K_{33R}/K_{33I})$ where K_{33R} and K_{33I} denote the real and imaginary parts respectively of the permeability K_{33}. It can be observed that the magnitude of the permeability is higher in the case of prolate cavities than for oblate cavities. Obviously, with the array of oblate spheroids, the solid phase is more compact in the plane orthogonal to the flow direction.

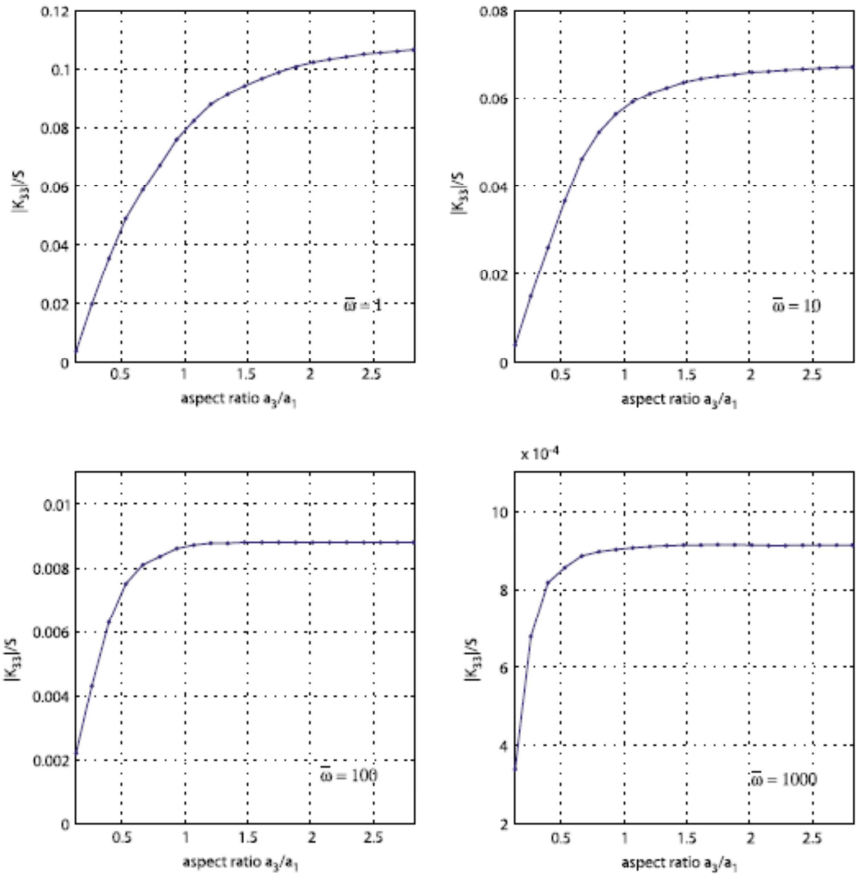

Fig. 7. Magnitude of the non-dimensional permeability, $|K_{33}|/S$, as a function of the aspect ratio for four values of the non-dimensional frequency $\overline{\omega} = 1, 10, 100, 1000$.

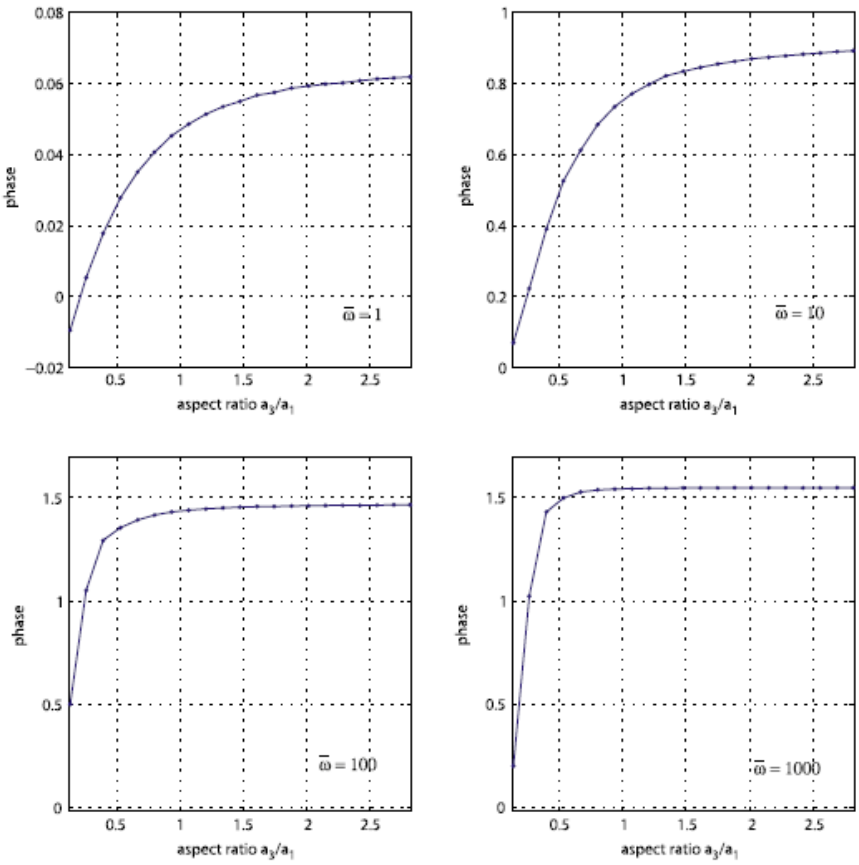

Fig. 8. The phase $\varphi = \arctan(K_{33R}/K_{33I})$ as a function of the aspect ratio for four values of the non-dimensional frequency $\overline{\omega} = 1, 10, 100, 1000$.

5. Conclusion

In this paper we have proposed a FFT based iterative scheme for computing the dynamic permeability of periodic porous media. This iterative scheme uses an exact expression of the dynamic Green tensor in the Fourier space. As a first validation of the approach, we compare our results with an existing closed-form solution in the case of a flow through a regular array of tubes. A validation with existing numerical data provided in the literature has also been proposed in the case of a flow through a regular array of rigid spheres. The FFT based method appears as an efficient alternative to other numerical methods for computing the dynamic permeability of porous solids. Indeed, this method is time saving, due to the use of the Fast Fourier Transform and memory saving, because there is no need of memory storage for interaction matrices as in Finite Element or Finite Difference methods. So, the use of that method for example in the case of elasticity problems allows us to treat geometries containing as many as 2048^3 pixels by using only 144 *Go* of memory. In addition, due to the regular discretization used in this method, it is well adapted for computing the dynamic permeability of samples whose microstructure is obtained from microtomography since in that case all data are provided on a regular framework. The use of such data is therefore straightforward for performing FFT computations.

Appendix. Computation of $\varphi(\underline{\xi}, \kappa)$ and $\underline{\underline{A}}^0(\underline{\xi}, \kappa)$

The strain rate field $\underline{\underline{\dot{\varepsilon}}}(\underline{\xi})$ computed from the velocity field $\underline{v}(\underline{\xi})$, given by the second relation in (17), is:

$$\begin{aligned}\underline{\underline{\dot{\varepsilon}}}(\underline{\xi}) &= \frac{i}{2}(\underline{v} \otimes \underline{\xi} + \underline{\xi} \otimes \underline{v}) \\ &= \frac{i}{2\mu_0|\underline{\xi}|^2(1-\kappa)}[(\boldsymbol{k}^\perp.\underline{f}) \otimes \underline{\xi} + \underline{\xi} \otimes (\boldsymbol{k}^\perp.\underline{f})] \\ &\quad + \frac{1}{1-\kappa}\Big[\underline{\eta}(\underline{\xi}).\boldsymbol{k} + \boldsymbol{k}.\underline{\eta}(\underline{\xi}) - 2\boldsymbol{k}(\underline{\eta}(\underline{\xi}) : \boldsymbol{k})\Big]. \qquad (A.1)\end{aligned}$$

The stress field is given by:

$$\begin{aligned}\underline{\underline{\sigma}}(\underline{\xi}) &= p(\underline{\xi})\underline{\underline{I}} + 2\mu_0[\underline{\underline{\dot{\varepsilon}}}(\underline{\xi}) - \underline{\underline{\eta}}(\underline{\xi})] \\ &= \frac{i}{|\underline{\xi}|^2(1-\kappa)}[(\boldsymbol{k}^\perp.\underline{f}) \otimes \underline{\xi} + \underline{\xi} \otimes (\boldsymbol{k}^\perp.\underline{f})] + \frac{i}{|\underline{\xi}|^2}\underline{f}.\underline{\xi}\underline{\underline{I}} \\ &\quad + \frac{2\mu_0}{1-\kappa}\Big[\underline{\eta}(\underline{\xi}).\boldsymbol{k} + \boldsymbol{k}.\underline{\eta}(\underline{\xi}) - 2\boldsymbol{k}(\underline{\eta}(\underline{\xi}) : \boldsymbol{k})\Big] - 2\mu_0\underline{\underline{\eta}}(\underline{\xi}) \\ &\quad + 2\mu_0\underline{\underline{\eta}}(\underline{\xi}) : \boldsymbol{k}\boldsymbol{I}. \qquad (A.2)\end{aligned}$$

The stress can be put into the form given by (19) with the following expressions for $\varphi(\underline{\xi}, \kappa)$ and $\underline{\underline{A}}^0(\underline{\xi}, \kappa)$:

$$\begin{cases} \varphi(\underline{\xi},\kappa) = \dfrac{i}{|\underline{\xi}|^2(1-\kappa)}[(\boldsymbol{k}^{\perp}.\underline{f})\otimes\underline{\xi} + \underline{\xi}\otimes(\boldsymbol{k}^{\perp}.\underline{f})] + \dfrac{i}{|\underline{\xi}|^2}\underline{f}.\underline{\xi}\boldsymbol{I} \\ \boldsymbol{\Delta}^0(\underline{\xi},\kappa) = -\dfrac{2\mu_0}{1-\kappa}\left[\boldsymbol{I}\underline{\otimes}\boldsymbol{k} + \boldsymbol{k}\underline{\otimes}\boldsymbol{I} - 2\boldsymbol{k}\otimes\boldsymbol{k}\right] \\ \qquad\qquad + 2\mu_0\mathbb{I} - 2\mu_0[\boldsymbol{I}\otimes\boldsymbol{k} + \boldsymbol{k}\otimes\boldsymbol{I}]. \end{cases} \tag{A.3}$$

By replacing $\boldsymbol{k}^{\perp}$ by $\boldsymbol{I} - \boldsymbol{k}$ in the first relation in (A.3) it is easy to recover the expression of $\varphi(\underline{\xi},\kappa)$ given by (20). By using the property:

$$\mathbb{I} = \boldsymbol{k}\otimes\boldsymbol{k} + \boldsymbol{k}^{\perp}\underline{\otimes}\boldsymbol{k}^{\perp} + \boldsymbol{k}\underline{\otimes}\boldsymbol{k}^{\perp} + \boldsymbol{k}^{\perp}\underline{\otimes}\boldsymbol{k} \tag{A.4}$$

in the second in (A.3) and after some simple algebraic manipulations, we obtain:

$$\begin{aligned} \boldsymbol{\Delta}^0(\underline{\xi},\kappa) = {} & \frac{2\mu_0\kappa}{1-\kappa}\left[\boldsymbol{k}^{\perp}\underline{\otimes}\boldsymbol{k} + \boldsymbol{k}\underline{\otimes}\boldsymbol{k}^{\perp}\right] \\ & + 2\mu_0[\boldsymbol{k}^{\perp}\otimes\boldsymbol{k}^{\perp} + \boldsymbol{k}^{\perp}\underline{\otimes}\boldsymbol{k}^{\perp} + \boldsymbol{I}\otimes\boldsymbol{I}]. \end{aligned} \tag{A.5}$$

Note that, in the above relation, the last term proportional to "$\boldsymbol{I}\otimes\boldsymbol{I}$" can be deleted since the Green tensor $\boldsymbol{\Delta}^0(\underline{\xi},\kappa)$ is applied to a deviatoric tensor $\eta(\underline{\xi})$. With this last operation, one recovers the expression given by (21).

References

[1] A.S. Sangani, A. Acrivos, Slow flow past periodic arrays of cylinders with application to heat transfer, Int. J. Multiphase Flow 8 (3) (1982) 193–206.
[2] A.S. Sangani, A. Acrivos, Slow flow through a periodic array of spheres, Int. J. Multiphase Flow 3 (4) (1982) 343–360.
[3] C.Y. Wang, Stokes flow through a rectangular array of circular cylinders, Fluid Dyn. Res. 29 (2001) 65–80.
[4] L. Borne, R. Chambon, J.-L. Auriault, Conforming finite element computations applied to a spatially periodic, harmonic Navier–Stokes problem, Int. J. Numer. Methods Fluids 5 (1985) 685–707.
[5] J. Barrere, J.P. Caltagirone, O. Gipouloux, Détermination numérique de la perméabilité en milieu poreux périodique tridimensionnel, C.R. Acad. Sci. Paris, Série II 310 (1990) 347–352.
[6] D. Cioranescu, P. Donato, H.I. Ene, Homogenization of the Stokes problem with non-homogeneous slip boundary conditions, Math. Methods Appl. Sci. 19 (11) (1996) 857–881.
[7] F.J. Alcocer, V. Kumar, P. Singh, Permeability of periodic porous media, Phys. Rev. E. 59 (1) (1999) 711–714.
[8] F.J. Alcocer, P. Singh, Permeability of periodic arrays of cylinders for viscoelastic flows, Phys. Fluids 14 (7) (2002) 2578–2581.
[9] E. Sawicki, Numerical investigation of the fluid flow through rotating porous media at both the microscopic scale and macroscopic scale, Ph.D. Thesis, University Joseph Fourier, Grenoble, France, 2004.
[10] T. Levy, Propagation of waves in a fluid-saturated porous elastic solid, Int. J. Engng. Sci. 17 (1979) 1005–1014.
[11] J.L. Auriault, Dynamic behaviour of porous medium saturated by a newtonian fluid, Int. J. Engng. Sci. 18 (1980) 775–785.
[12] R. Burridge, J.B. Keller, Poroelasticity equations derived from microstructure, J. Acoust. Soc. Am. 70 (4) (1981) 1140–1146.
[13] D.L. Johnson, J. Koplik, R. Dashen, Theory of dynamic permeability and tortuosity in fluid-saturated porous media, J. Fluid Mech. 176 (1987) 379–202.
[14] M.Y. Zhou, P. Sheng, First-principles calculations of dynamic permeability in porous media, Phys. Rev. B 39 (16) (1989) 12027–12039.
[15] A.M. Chapman, J.J.L. Higdon, Oscillatory Stokes flow in periodic porous media, Phys. Fluids A 4 (10) (1992) 2099–2116.
[16] D.M.J. Smeulders, R.L.G.M. Eggels, M.E.H. Van Dongen, Dynamic permeability reformulation of theory and new numerical and experimental data, J. Fluid Mech. 245 (1992) 211–227.
[17] C. Perrot, F. Chevillotte, R. Panneton, Dynamic viscous permeability of an open-cell aluminum foam Computations versus experiments, J. Appl. Phys. 318 (2008) 024909.
[18] I. Malinouskaya, V.V. Mourzenko, J.-F. Thovert, P.M. Adler, Wave propagation through saturated porous media, Phys. Rev. E 77 (2008) 066302.
[19] V. Monchiet, G. Bonnet, G. Lauriat, A FFT-based method to compute the permeability induced by a Stokes slip flow through a porous medium, C.R. Mec. 337 (4) (2009) 192–197.
[20] H. Moulinec, P. Suquet, A fast numerical method for computing the linear and nonlinear mechanical properties of composites, C. R. Acad. Sci. 318 (11) (1994) 1417–1423.
[21] C. Canuto, M.Y. Hussaini, A. Quarteroni, T.A. Zang, Spectral Methods, Springer, 2007.
[22] T. Kanit, S. Forest, I.a Galliet, V.a Mounoury, D. Jeulin, Determination of the size of the representative volume element for random composites. Statistical and numerical approach, Int. J. Solid Struct. 40 (13–14) (2003) 3647–3679.
[23] H.I. Ene, E. Sanchez-Palencia, Equations and surface phenomena for the flow in a porous medium, J. Mec. 14 (1) (1975) 73–108.
[24] J.L. Auriault, E. Sanchez-Palencia, Study of macroscopic behavior of a deformable porous medium, J. Mec. 16 (4) (1977) 575–603.
[25] J.L. Auriault, C. Boutin, C. Geindreau, Homogénéisation de phénomènes couplés en milieu hétérogène 2. Quasi-statique et dynamique des milieux poreux, Hermès Sciences, 2009.
[26] E. Sanchez-Palencia, Nonhomogeneous Media and Vibration Theory, in: Lecture Notes in Physics, vol. 127, Springer, Berlin, 1980.
[27] K. Bhattacharya, P.M. Suquet, A model problem concerning recoverable strains of shape-memory polycrystals, Proc. Roy. Soc. London A 461 (2005) 2797–2816.
[28] G. Bonnet, Effective properties of elastic periodic composite media with fibers, J. Mech. Phys. Solids 55 (2007) 881–899.
[29] J-C. Michel, H. Moulinec, P. Suquet, A computational scheme for linear and non-linear composites with arbitrary phase contrast, Int. J. Numer. Methods Eng. 52 (2001) 139–160.
[30] V. Monchiet, G. Bonnet, A polarization based FFT iterative scheme for computing the effective properties of elastic composites with arbitrary contrast, Int. J. Num. Methods Eng. 89 (11) (2012) 1419–1436.
[31] C. Boutin, Dynamique des milieux poreux saturés déformables — Fonction de Green - Perméabilité dynamique, Ph.D. Thesis, University Joseph Fourier, Grenoble, France, 1987.
[32] P. Sheng, M.Y. Zhou, Dynamic permeability in porous media, Phys. Rev. Lett. 61 (14) (1988) 1591–1594.